J. Fluid Mech. (1979), *vol.* 93, *part* 3, *pp.* 529–548
Printed in Great Britain

On the flow around a buoyant cylinder within a rapidly rotating horizontal cylindrical container

By ROGER F. GANS

Department of Mechanical and Aerospace Sciences,
University of Rochester, New York 14627

(Received 2 June 1978 and in revised form 15 January 1979)

Steady flow in a cylinder of finite length rotating rapidly at right angles to the earth's gravity and containing a rigid cylindrical float is found under the assumption of small viscosity. The float is modelled by a 'rigid free surface'. The major new result is a prediction of the rotation rate of the interface, which differs by a factor of $O(E^{\frac{1}{4}})$ from those given by Greenspan (1976) and Wood (1977) for a rigid interface in an infinitely long cylinder. The difference is accounted for by the appearance of Stewartson layers on the inner boundary in the finite case. The result is supported by an experiment of my own, and is not in conflict with the experimental results given by Greenspan.

Some additional experimental observations are reported: a comparison of free and rigid surface rotation rates; and a brief description of the spin-up from rest.

1. Introduction

The present paper is an extension of an earlier paper (Gans 1977, hereafter referred to as RFG). In that paper I calculated the flow of an incompressible viscous fluid partially filling a rapidly rotating cylindrical container. The container was supposed to rotate about its principal symmetry axis, held horizontal. The flow was assumed to be nearly a solid rotation, differing because of gravity acting at the cylindrical free surface separating the liquid from the void. (The object of this calculation was to find the steady-state flow that may underlie a number of exciting time-dependent phenomena described in RFG and references cited therein.)

The calculation used an amplitude expansion in powers of $\epsilon = g/\Omega^2 a$, where g, Ω and a denote gravitational acceleration, container rotation rate and radius, respectively. At each power of ϵ I used a boundary-layer analysis based on the smallness of E, $= \nu/\Omega a^2$, where ν denotes the kinematic viscosity.

The first-order (in ϵ) solution is essentially the same as that found by Phillips (1960), with the addition of boundary layers to satisfy viscous boundary conditions. The second-order analysis was directed at calculating the axisymmetric part of the flow, with a view to predicting the rotational speed of the interface: a dependent variable susceptible to measurement.

Subsequently Whiting (1978) measured this interface rotation rate. His data disagree sharply with the theoretical prediction. The data give a difference between container and interface rotation rate roughly seven times larger than I predicted in RFG.

Greenspan (1976) and Wood (1977) addressed (in different ways, with different

0022–1120/79/4274–7070 $02.00

results, which I will discuss briefly below) a similar problem: flow in a rapidly rotating cylinder like mine, the void space of which is occupied by a buoyant rigid straw. This model is in essence a 'rigid free surface'. Both Greenspan and Wood calculated the rotation rate of the straw and found it to differ from the container rate by an amount not $O(\epsilon^2)$ as in RFG, but $O(\epsilon^2 E^{-\frac{1}{2}})$. This qualitative difference is a consequence of the change in boundary condition. On a free surface the shear stresses must vanish; on a rigid free surface non-axisymmetric velocity components must vanish because the fluid cannot slip relative to the surface. In addition the net torque on the straw must vanish.

Whiting's data (*op. cit.*) lie between the two predictions; Greenspan's data is 'in fair agreement with theory' (1976, p. 342). I will discuss a possible interpretation of this below.

There is a flaw in both Greenspan and Wood: the calculations reported are strictly two-dimensional. I showed in RFG that the nature of the swirl away from the radial boundaries is controlled by Ekman suction on the end walls. I was able to construct an argument based on mass conservation which showed that the interior swirl, by which I mean the azimuthal component of the azimuthally averaged velocity field, has a component proportional to the inverse fifth power of the radial co-ordinate, and that there could be no component proportional to the inverse first power: no potential vortex.

A second consequence of the existence of end walls was the possibility of Stewartson layers; axisymmetric boundary layers with dimensionless thicknesses $O(E^{\frac{1}{3}})$ and $O(E^{\frac{1}{4}})$ admitting axial flow and axial dependence. Whiting's experiments clearly demonstrate axial flow at the inner interface. This axial flow varies in the axial direction. The swirl at the interface, on the other hand, is independent of axial direction, in agreement with all three models.

I remarked that the results of Greenspan (1976) and Wood (1977) are not identical. The difference is not discussed by Wood, who states that 'a formula. . . essentially the same as [that of Greenspan] follows very simply [from the analysis]' (1977, p. 1953). Discussion of the difference seems appropriate in this introduction, especially since Wood's formulation is simpler than Greenspan's and would provide a useful tool to aid in the understanding of the physics.

Wood's formulation balances the energy dissipation within a boundary layer surrounding the straw against the work done on the boundaries of that boundary layer. Because the straw is torque free, work is contributed only by stresses at the edge of the inviscid region: a radius equal to the core radius plus the boundary-layer thickness. The relevant integrals can be most easily derived by taking the inner product of the momentum equation and the velocity and integrating over the boundary layer [cf. Landau & Lifschitz 1959, § 16]. Using the conditions of two-dimensionality and no flow across the boundary-layer edges leads to an integral expression:

$$\int_V \left[u_r^2 + \frac{1}{r^2}(v_\phi + u)^2 + \frac{1}{2r^2}(u_\phi + rv_r - v)^2 \right] dv = \int_S \left[uu_r + \frac{v}{2r}(u_\phi + rv_r - v) \right] dS, \quad (1.1)$$

where u and v denote radial and azimuthal velocity components, r and ϕ radial and azimuthal co-ordinates, subscripts partial derivatives, V and S the volume and outer (fluid side) surface of the boundary layer.

I will define interior and boundary-layer components of the velocities, and distinguish the former by a caret and the latter by a tilde:

$$u = \hat{u} + \tilde{u}; \quad v = \hat{v} + \tilde{v}. \tag{1.2}$$

The interior components do not change significantly across the boundary layer; the boundary-layer components become exponentially small outside the boundary layer, and have large radial derivatives within the boundary layer.

I will also use an overbar to denote ϕ averages, or axisymmetric components:

$$\bar{u} = \frac{1}{2\pi}\int_0^{2\pi} u\, d\phi; \quad \bar{v} = \frac{1}{2\pi}\int_0^{2\pi} v\, d\phi. \tag{1.3}$$

Wood's interior azimuthal velocity can be written in the form

$$\hat{v} = ar + b/r + \epsilon V(r, \phi),$$

where he uses an ϵ to denote the small dimensionless displacement of the straw axis from the container axis. There is no $\hat{u}$ given; were there one, conservation of mass shows it must be $O(\epsilon)$. Thus the right-hand side of (1.1), which can contain only interior (non-boundary-layer) components, becomes

$$-\frac{1}{2}\int_S \left[\left(a + \frac{b}{r^2}\right)\frac{b}{r^2} + O(\epsilon^2)\right] dS. \tag{1.4}$$

The left-hand side is dominated by the radial derivative of the boundary-layer azimuthal velocity, so that, in Wood's formulation, equation (1.1) reduces to

$$\int_V \tilde{v}_r^2\, dv = -\int_S \left(a + \frac{b}{r^2}\right)\frac{b}{r^2} dS. \tag{1.5}$$

By assuming that a is nearly the container rotation rate, $b/r^2 \ll a$ and using $\tilde{v}_r$ taken from Wood (1957), Wood finds that b/r^2 is $O(\epsilon^2 E^{-\frac{1}{2}})$ and that

$$\Omega_s \sim 1 - \frac{\alpha^2}{4\sqrt{(2)}\, E_G^{\frac{1}{2}}}, \tag{1.6}$$

where $\alpha = g/\Omega^2 ac$ and $E_G = \nu/\Omega a^2 c^2$ are the small parameters used by Greenspan, c is the ratio of straw radius to container radius, and Ω_s is the rotation rate of the straw divided by that of the container.

I call the term $\alpha^2[4\sqrt{(2)}E_G^{\frac{1}{2}}]^{-1}$ the retrograde rotation. It is what an observer sees viewing an experimental cylinder which is illuminated by a stroboscope flashing at the container rotation rate. It is dominated, in Wood (1977), by the interior potential vortex.

Greenspan obtains the retrograde rotation by demanding that there be no net torque on the inner surface. (This condition is assumed by Wood, but not demonstrated.) The net torque in the axial direction can be written

$$T = \int_{S'} r\mu \left[\frac{1}{r}u_\phi + v_r - \frac{v}{r}\right] dS, \tag{1.7}$$

where S' is the surface of the straw. On the surface of the straw $u \equiv 0$, there is no contribution from the solid rotation, and to leading order

$$1 - \Omega_s = \frac{r_i}{\Omega}\overline{\tilde{v}_r}, \tag{1.8}$$

where r_i is the radius of the straw. This value is twice that given by Wood.

I prefer to accept the Greenspan (1976) result, primarily because that analysis is more detailed. This paper is not the place for a detailed analysis of the differences, so I will restrict myself to two comments.

1. There appear to be no simple errors in algebra or typography. Either result can be reproduced using the two-dimensional analogues of the velocity fields I compute below, under the appropriate hypothesis.

2. Woods' result *may* be non-uniform. The right-hand side of 1.5 is formally $O(1)$. It is constructed by neglecting terms which are $O(\epsilon)$ and terms which are $O(\delta)$, where δ is used here (only) to denote a boundary-layer thickness. Since the result is $O(\epsilon^2 E^{-\frac{1}{2}})$, there is a possibility that some terms have been neglected that ought not to have been neglected. A similar difficulty does not arise in Greenspan's analysis.

Both results depend on a strictly two-dimensional flow which cannot be realized in a finite container. In a 'long' container, the Stewartson layers expand to fill the container. In a 'short' container the Stewartson layers are truly thin boundary layers. Both Greenspan and Whiting reported experiments in short containers, with aspect ratios $\lambda = 1{\cdot}25$ and $1{\cdot}15$ respectively.

In this paper, I present a calculation leading to the prediction of the rotation rate of the straw and experimental results for a particular straw. I find its departure from co-rotation to be $O(\epsilon^2 E^{-\frac{1}{4}})$. The difference arises from the three-dimensionality of the calculated flow. This three-dimensionality is forced by the assumption of a cylinder of finite length.

The analysis parallels that in RFG. In §§ 2 and 3, I have constructed a formulation and presented some calculations in an effort to make this paper reasonably self-contained.

Section 4 compares both theoretical predictions to the experimental data in HPG, and to experimental data from my laboratory. The latter experiment is described. Some experimental observations of phenomena outside the reach of the present theory, such as the non-ideal free surface data and spin-up from rest, are described as well in § 4.

2. Formulation

All analyses agree that the lowest-order effect of gravity is to cause the core to be displaced from the centre, primarily in a downward direction, a distance proportional to ϵ. Whiting's (1978) measurement agrees with the prediction, which is independent of the nature of the interface. Thus, a system of co-ordinates centred in the container leads to serious difficulties in an analysis of boundary layers 'on' the interface.

Greenspan (1976) circumvented this difficulty in an elegant fashion by introducing a stream function and a complex transformation mapping the non-concentric circles into concentric circles: an adaption of a method used by Wood (1957). RFG resolved the difficulty by using two sets of co-ordinates and matching velocities at intermediate radii, near neither the outer wall of the container nor the interfacial region. I will use the latter approach here, as it facilitates consideration of axial variations.

Details of the co-ordinate transformation are given in RFG. In essence one supposes that there are two co-ordinate systems $\mathbf{x}$ and $\bar{\mathbf{x}}$, called the core and container co-ordinates, respectively, separated by an (unknown) small distance $\delta\epsilon a$. One finds δ such that the location of the interface in dimensionless cylindrical core co-ordinates,

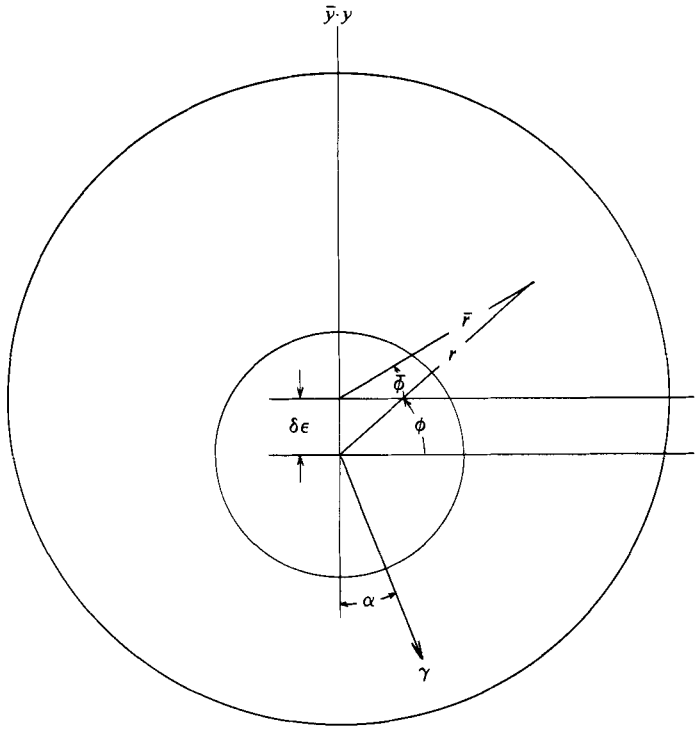

FIGURE 1. Sketch of the two co-ordinate systems.

$r = aC(\phi, z)$, has no component singly periodic in ϕ. (Such a component corresponds to a translation of the core.) Then

$$r = [c + \epsilon^2 \chi]\, a \tag{2.1}$$

is the location of the boundary in core co-ordinates, and, to the order to be assessed here, one can substitute $r = ac$ into the expressions for the dependent variables on the interface and not need to include radial derivatives of the dependent variables.

In the sequel the following non-dimensionalization is used. I set $\mathbf{r} = a\mathbf{r}'$ and $\mathbf{v} = \Omega a \mathbf{v}'$, and substitute these into the differential equations and boundary conditions. Four non-dimensional numbers appear: ϵ and E, defined in § 1, c, the dimensionless radius of the straw defined by (2.1), and λ, the length to diameter ratio of the container. After non-dimensionalization the primes are dropped as superfluous.

Because the interface is supposedly rigid, C will be constant (equal to c). The same transformation is made as in RFG, but the condition determining δ (and the angle α between the gravity and core displacement vectors) is that the net force on the core (or straw) is zero.

Formally, the Cartesian transformation, in cylindrical co-ordinates, is

$$\bar{r}\cos\bar{\phi} = r\cos\phi, \quad \bar{r}\sin\bar{\phi} = r\sin\phi - \delta\epsilon. \tag{2.2}$$

The two systems share a common axial (z) co-ordinate.

The line joining the two systems is not necessarily vertical (parallel to gravity). Thus the vector parallel to gravity is written

$$\boldsymbol{\gamma} = \sin\alpha\mathbf{i} - \cos\alpha\mathbf{j}, \tag{2.3}$$

where **i** and **j** are Cartesian unit vectors in either co-ordinate system, and α is an (unknown) angle. These are all shown in figure 1.

The radial and azimuthal velocity components are written $u(r, \phi, z)$, $v(r, \phi, z)$ and $\bar{u}(\bar{r}, \bar{\phi}, \bar{z})$, $\bar{v}(\bar{r}, \bar{\phi}, \bar{z})$. The matching condition, derived in RFG, is

$$u(\rho, \theta, \zeta) - \bar{u}(\rho, \theta, \zeta) = -\tfrac{1}{2}\delta\epsilon\left[\left(\sin\theta\frac{\partial}{\partial\rho} + \cos\theta\frac{1}{\rho}\frac{\partial}{\partial\theta}\right)(u+\bar{u}) - \frac{1}{\rho}\cos\theta(v+\bar{v})\right] + O(\epsilon^3), \tag{2.4a}$$

$$v(\rho, \theta, \zeta) - \bar{v}(\rho, \theta, \zeta) = -\tfrac{1}{2}\delta\epsilon\left[\left(\sin\theta\frac{\partial}{\partial\rho} + \cos\theta\frac{1}{\rho}\frac{\partial}{\partial\rho}\right)(v+\bar{v}) + \frac{1}{\rho}\cos\theta(u+\bar{u})\right] + O(\epsilon^3). \tag{2.4b}$$

This condition has been developed by: (1) expanding u and v in a Taylor expansion about $(r, \phi, z) = (\rho, \theta, \zeta)$ and $\bar{u}$ and $\bar{v}$ about $(\bar{r}, \bar{\phi}, \bar{z}) = (\rho, \theta, \zeta)$; (2) equating the two representations at a single physical point midway between the two points

$$(r, \phi, z) = (\rho, \theta, \zeta) \quad \text{and} \quad (\bar{r}, \bar{\phi}, \bar{z}) = (\rho, \theta, \zeta).$$

I have introduced the extra notation with the aim of making this clear.

Because attention is directed at the inner interface, most of calculations will be carried out in core co-ordinates. Some results will be given in both systems, to make it easy to compare with Phillips, who worked in container co-ordinates.

It is convenient to separate out a component of a solid rotation by writing the velocity as

$$\mathbf{v} = r\hat{\mathbf{e}}_\phi + \epsilon\mathbf{u}, \tag{2.5}$$

and the pressure as

$$P = P_0 + \tfrac{1}{2}r^2 + \epsilon\boldsymbol{\gamma}\,.\,\mathbf{r} + \epsilon p \tag{2.6}$$

with similar expressions in the barred co-ordinates. Here P_0 is a constant and $\hat{\mathbf{e}}_\phi$ is a unit vector in the ϕ direction. The substitution of (2.5) and (2.6) into the general equations of motion yields equations for **u** and p, which, assuming steady motions in the laboratory frame, are

$$\mathbf{u}_{\phi_1} + 2\hat{\mathbf{e}}_z \times \mathbf{u} + \epsilon\mathbf{u}\,.\,\nabla\mathbf{u} + \nabla p = E\nabla^2\mathbf{u},$$
$$\nabla\,.\,\mathbf{u} = 0. \tag{2.7}$$

(As usual $\mathbf{u}_{\phi_1}$ means the partial derivative with respect to ϕ of the components of **u** only.)

The boundary conditions for the set (2.7) are the usual no-slip conditions on the solid boundaries. On the rigid free surface one also has no-slip conditions, but, as the straw is free to rotate and translate, there are additional conditions: the net force and torque on the straw must vanish [cf. Greenspan 1976]. These conditions determine the location and rotation rate of the straw, respectively.

As the straw can move only in the x and y directions, the fluid-generated force on the straw can have only x and y components. Similarly, the fluid-generated torque has only a z component. The forces and torque may be written in terms of the stresses:

$$\sigma_{rr} = -P_0 - \tfrac{1}{2}r^2 - \epsilon\boldsymbol{\gamma}\,.\,\mathbf{r} - \epsilon p + 2E\epsilon u_r; \quad \sigma_{r\phi} = \epsilon E\left(\frac{1}{r}u_\phi + v_r - \frac{v}{r}\right).$$

The force conditions are:

$$\int_0^{2\pi} d\phi\{\cos\phi\sigma_{rr} - \sin\phi\sigma_{r\phi}\} = 0; \quad \int_0^{2\pi} d\phi\{\cos\phi\sigma_{r\phi} + \sin\phi\sigma_{rr}\} = 0; \tag{2.8}$$

and the torque condition is

$$\int_0^{2\pi} d\phi\,[r\sigma_{r\phi}] = 0. \tag{2.9}$$

In equilibrium the surface of the straw can have only constant azimuthal velocity so that the no-slip condition may be written

$$u = 0 = w, \quad v = c[\Omega_s - 1], \tag{2.10}$$

where Ω_s is the dimensionless rotation rate of the straw, to be determined (from the torque balance) during the course of the analysis.

One notes that $\epsilon\boldsymbol{\gamma}\cdot\mathbf{r}$ is the only inhomogeneous term in the problem. This was anticipated in the substitutions (2.5) and (2.6), and I use this to motivate the construction of an expansion of the form

$$\mathbf{u} = \mathbf{u}^{(0)} + \epsilon\mathbf{u}^{(1)} + \ldots, \quad p = p^{(0)} + \epsilon p^{(1)} + \ldots . \tag{2.11}$$

Within this expansion it is necessary to divide the solutions into interior and boundary-layer parts as

$$\mathbf{u}^{(n)} = \hat{\mathbf{u}}^{(n)} + \tilde{\mathbf{u}}^{(n)}, \quad p^{(n)} = \hat{p}^{(n)} + \tilde{p}^{(n)}, \tag{2.12}$$

using the caret for interior flow and the tilde for boundary-layer flows.

As

$$\boldsymbol{\gamma}\cdot\mathbf{r} = r[\sin\alpha\cos\phi - \cos\alpha\sin\phi],$$

the $n = 0$ solutions will be singly-periodic in ϕ, and, by nonlinear interaction, these will force doubly-periodic and axisymmetric $n = 1$ solutions. Only the latter will be of interest here, as the primary goal is to calculate the rotation rate of the straw.

The result of putting (2.11) and (2.12) into the no-slip conditions on the solid boundaries is that

$$\mathbf{n}\cdot(\hat{\mathbf{u}}^{(n)} + \tilde{\mathbf{u}}^{(n)}) = 0, \quad \mathbf{n}\times(\hat{\mathbf{u}}^{(n)} + \tilde{\mathbf{u}}^{(n)}) = 0; \tag{2.13}$$

the former analogous to an Ekman matching condition, and the latter the no-slip condition determining the boundary-layer solutions; $\mathbf{n}$ is a vector normal to the surface.

[In general $\mathbf{n}\cdot\tilde{\mathbf{u}}^{(n)}$ will be of the order of the boundary-layer thickness smaller than $\mathbf{n}\cdot\hat{\mathbf{u}}^{(n)}$, and inclusion of this term in the normal boundary condition carries with it an implication regarding ordering. The next contribution to such a match (the first omitted term) will be that contributed by $\mathbf{n}\cdot\hat{\mathbf{u}}^{(n+2)}$, as the $n+1$ term will have different symmetry in its azimuthal dependence. Thus the condition as written in the first of (2.13) implies that ϵ is small compared to the square root of the boundary-layer thickness. As the thinnest boundary layer is of thickness $E^{\frac{1}{2}}$, $\epsilon \ll E^{\frac{1}{2}}$.]

Making use of the periodicity information to simplify the expressions (Ω_s must be constant) gives, for the no-slip conditions on the straw:

$$\left.\begin{aligned} [\hat{u}^{(n)} + \tilde{u}^{(n)}] = 0 = [\hat{w}^{(n)} + \tilde{w}^{(n)}], \\ [\hat{v}^{(0)} + \tilde{v}^{(0)}] = 0, \quad [\overline{\hat{v}^{(1)}} + \overline{\tilde{v}^{(1)}}] = (\Omega_s - 1)c, \end{aligned}\right\} \tag{2.14}$$

where the reader will recall that the overbar denotes a ϕ average, e.g.

$$\overline{v^{(1)}} = \frac{1}{2\pi}\int_0^{2\pi} v^{(1)}\,d\phi.$$

Substitution of (2.5), (2.6) and the stress expressions into the force equations gives

$$0 = \int_{-\lambda}^{\lambda} dz \int_0^{2\pi} d\phi \left\{ -\sin\phi \left[\epsilon E \left(\frac{1}{r} u_\phi + v_r - \frac{1}{r} v \right) \right] + \cos\phi [-P_0 - \tfrac{1}{2}c^2 - \epsilon \boldsymbol{\gamma} \cdot \mathbf{r} - \epsilon p + 2E\epsilon u_r] \right\},$$

$$0 = \int_{-\lambda}^{\lambda} dz \int_0^{2\pi} d\phi \left\{ \cos\phi \left[\epsilon E \left(\frac{1}{r} u_\phi + v_r - \frac{1}{r} v \right) \right] + \sin\phi [-P_0 - \tfrac{1}{2}c^2 - \epsilon \boldsymbol{\gamma} \cdot \mathbf{r} - \epsilon p + 2E\epsilon u_r] \right\}, \tag{2.15}$$

which can be simplified using the expressions (2.11) and (2.12) and symmetry considerations. First, the integral over the constant terms, $P_0 + \frac{1}{2}c^2$, will vanish, so that all the leading terms in the integrals will be $O(\epsilon)$, involving $\mathbf{u}^{(0)}$, $p^{(0)}$ and $\boldsymbol{\gamma} \cdot \mathbf{r}$. There will be no contribution from $\mathbf{u}^{(1)}$, $p^{(1)}$ because these functions are either axisymmetric or doubly-periodic in azimuth and will not contribute to the integrals. Thus one can replace u, v and p by $u^{(0)}$, $v^{(0)}$ and $p^{(0)}$ with an error ϵ^2 smaller than the terms retained.

The no-slip condition can be used to further reduce the problem, by noting that $u^{(0)}$ and $\hat{v}_r^{(0)}$ vanish on the straw, leading to reduced force conditions

$$\int_{-\lambda}^{\lambda} \int_0^{2\pi} d\phi \{ -\sin\sigma\epsilon E v_r^{(0)} - \epsilon \cos\phi [\boldsymbol{\gamma} \cdot \mathbf{r} + p^{(0)} - 2E u_r^{(0)}] \} = 0;$$

$$\int_{-\lambda}^{\lambda} \int_0^{2\pi} d\phi \{ \cos\phi \epsilon E v_r^{(0)} - \epsilon \sin\phi [\boldsymbol{\gamma} \cdot \mathbf{r} + p^{(0)} - 2E u_r^{(0)}] \} = 0. \tag{2.16}$$

Away from the end walls (where straw-wall–fluid interaction is unlikely to be amenable to analysis in any case) $\mathbf{u}^{(0)}$ is strictly two-dimensional, so that $v^{(0)} = 0 = u^{(0)}$ implies $u_r^{(0)} = 0$. Only $v_r^{(0)}$ does not vanish, and it will be dominated by $\tilde{v}_r^{(0)}$, which will be $E^{-\frac{1}{2}}$ larger than $\hat{v}_r^{(0)}$. The force equations are then

$$\int_0^{2\pi} d\phi \{ \sin\phi E \tilde{v}_r^{(0)} + \cos\phi [\boldsymbol{\gamma} \cdot \mathbf{r} + p^{(0)}] \} = 0,$$

$$\int_0^{\pi} d\phi \{ \cos\phi E \tilde{v}_r^{(0)} - \sin\phi [\boldsymbol{\gamma} \cdot \mathbf{r} + p^{(0)}] \} = 0, \tag{2.17}$$

where terms of $O(1)$ and $O(E^{\frac{1}{2}})$ are retained, consistent with the earlier ordering of the matching conditions.

A similar series of arguments regarding symmetry lead to a reduced torque condition (formally identical to the second-order shear condition in RFG):

$$\overline{v_r^{(1)}} - \frac{1}{c} \overline{v^{(1)}} = 0. \tag{2.18}$$

As $\overline{v^{(1)}}$ involves Ω_s, equation (2.18) will become an equation for Ω_s.

3. Calculations

The retrograde rotation has three components: (1) an interior flow arising from a balance of Ekman suctions on $z = \pm\lambda$; (2) a forced boundary layer of thickness $E^{\frac{1}{2}}$ arising from the particular solution to the boundary-layer equations; and (3) a set of Stewartson layers of thickness $E^{\frac{1}{4}}$ and $E^{\frac{1}{3}}$. The first of these components is unchanged from RFG. The second was negligible in the context of RFG; it cannot be neglected here. The third is modified by the prominence of the second.

Some discussion of the equation in question will make these statements clearer. If one examines the Navier–Stokes equations under the hypothesis that radial derivatives are large compared to axial and azimuthal derivatives, and further takes a ϕ average, one finds that the azimuthal component of these equations becomes, on retaining dominant terms and subtracting the non-boundary-layer part:

$$E\tilde{v}^{(1)}_{rr} = \frac{1}{r}\overline{u^{(0)}(r\tilde{v}^{(0)})}_r + \frac{1}{r}\overline{\tilde{u}^{(0)}(r\hat{v}^{(0)})}_r. \tag{3.1}$$

Within the boundary layer $u^{(0)}[=\hat{u}^{(0)}+\tilde{u}^{(0)}]$ will be $E^{\frac{1}{2}}$ smaller than $\tilde{v}^{(0)}$, and $\tilde{v}^{(1)}_r$ will be $E^{-\frac{1}{2}}$ larger than $\tilde{v}^{(0)}$. The first term on the right-hand side of (3.1) will be of the order of $[\tilde{v}^{(0)}]^2$. The second term will be of the order of $E^{\frac{1}{2}}\tilde{v}^{(0)}\hat{v}^{(0)}$. All of these terms vary radially in a scale of $E^{\frac{1}{2}}$, so that the particular solution to (3.1) will be of the same magnitude as the right-hand side.

If the surface is free, then $\tilde{v}^{(0)}_r$ will be of the same order as $\hat{v}^{(0)}_r$ [which is $O(1)$], and $\tilde{v}^{(0)} = O(E^{\frac{1}{2}})$. Thus the right-hand side of (3.1), and hence its particular solution, will be $O(E)$ and negligible. However, if the surface is rigid, then $\tilde{v}^{(0)}$ will be of the same order as $\hat{v}^{(0)}$, $O(1)$, and the right-hand side of (3.1) will be $O(1)$.

In either case the boundary condition on $\overline{v^{(1)}}$ involves shear. As will be seen below, the shear balance takes place in an $E^{\frac{1}{4}}$ layer, and is among an interior $[O(1)]$ solution, the particular solution and the $E^{\frac{1}{4}}$ layers. Denoting these magnitudes by A_I, A_p and $A_{\frac{1}{4}}$ one has, symbolically,

$$\frac{A_I}{c} + \frac{A_p}{E^{\frac{1}{2}}} + \frac{A_{\frac{1}{4}}}{E^{\frac{1}{4}}} = 0.$$

If $A_p \lesssim E^{\frac{1}{2}}$ (as in the free surface case) $A_{\frac{1}{4}} \sim E^{\frac{1}{4}}$ and $\Omega_s \sim A_I/c$. If $A_p = O(1)$, as in the rigid surface case, then $A_{\frac{1}{4}} \sim E^{-\frac{1}{4}}$ and $\Omega_s \sim A_{\frac{1}{4}}/c \sim E^{-\frac{1}{4}}/c$.

The remainder of this section presents such calculations as are necessary to make these arguments quantitative.

3.1. *The linear solution*

To begin one needs to form the nonlinear term, for which one needs the linear solution, $\mathbf{u}^{(0)}$. The differential equations governing $\mathbf{u}^{(0)}$, $p^{(0)}$ are obtained from (2.7) by replacing $\mathbf{u}$, p by $\mathbf{u}^{(0)}$, $p^{(0)}$ and letting $\epsilon \to 0$. General solutions away from the end walls (end-wall boundary layers can be added; they are identical to those described in RFG) are:

$$\hat{u}^{(0)} = -\left[A_s + \frac{B_s}{3r^2}\right]\cos\phi + \left[A_c + \frac{B_c}{3r^2}\right]\sin\phi,$$

$$\hat{v}^{(0)} = \left[A_s - \frac{B_s}{3r^2}\right]\sin\phi + \left[A_c - \frac{B_c}{3r^2}\right]\cos\phi,$$

$$\hat{p}^{(0)} = \left[A_s r + \frac{B_s}{r}\right]\sin\phi + \left[A_c r + \frac{B_c}{r}\right]\cos\phi;$$

$$\tilde{u}^{(0)} = \frac{(2E)^{\frac{1}{2}}}{2c}\exp R[(\tilde{A}+\tilde{B})\cos(R+\phi) - (\tilde{A}-\tilde{B})\sin(R+\phi)],$$

$$\tilde{v}^{(0)} = \exp R[\tilde{A}\cos(R+\phi) + \tilde{B}\sin(R+\phi)],$$

$$\tilde{p}^{(0)} = -(2E)^{\frac{1}{2}}\exp R[(\tilde{A}-\tilde{B})\cos(R+\phi) + (\tilde{A}+\tilde{B})\sin(R+\phi)]. \tag{3.2}$$

Here A_s, B_s, A_c, B_c, $\tilde{A}$ and $\tilde{B}$ are constants, the leading order of which will not exceed unity, and

$$R = (c-r)/(2E)^{\frac{1}{2}}. \tag{3.3}$$

Similar expressions apply in container co-ordinates with R replaced by $(\bar{r}-1)(2E)^{-\frac{1}{2}}$, c replaced by unity in the expression for $\mathbf{u}$ and the appropriate sign corrections made. These are given in RFG. If we use the symbols to stand for the constants in the interior solutions, with an overbar to denote container representations, the matching conditions are

$$\bar{A}_s = A_s + \delta, \quad \bar{A}_c = A_c, \quad \bar{B}_s = B_s, \quad \bar{B}_c = B_c, \tag{3.4}$$

which eliminate the barred constants (cf. RFG).

The no-slip condition on $\bar{r} = 1$ eliminates $\bar{\tilde{A}}$ and $\bar{\tilde{B}}$ in terms of the barred interior constants, hence the unbarred interior constants:

$$\bar{\tilde{A}} = -A_c + \tfrac{1}{3}B_c, \quad \bar{\tilde{B}} = -A_s + \tfrac{1}{3}B_s - \delta. \tag{3.5}$$

The normal condition ($\bar{u} = 0$) on $\bar{r} = 1$ allows one to eliminate A_s and A_c:

$$\left.\begin{aligned} A_s &= -\delta - \frac{1-2e}{(1-e)^2+e^2}\tfrac{1}{3}B_s - \frac{2e}{(1-e)^2+e^2}\tfrac{1}{3}B_c; \\ A_c &= \frac{2e}{(1-e)^2+e^2}\tfrac{1}{3}B_s - \frac{1-2e}{(1-e)^2+e^2}B_c; \end{aligned}\right\} \tag{3.6}$$

where $e = (\frac{1}{2}E)^{\frac{1}{2}}$ and the expression (3.6) is a formal one, only valid to $O(e)$.

The no-slip condition on the inner ($r = c$) boundary serves to eliminate $\tilde{A}$ and $\tilde{B}$:

$$\left.\begin{aligned} \tilde{A} &= \delta + \frac{(1-2e)c^2 + (1-e)^2 + e^2}{c^2[(1-e)^2+e^2]}\tfrac{1}{3}B_s + \frac{2e}{(1-e)^2+e^2}\tfrac{1}{3}B_c, \\ \tilde{B} &= -\frac{2e}{(1-e)^2+e^2}\tfrac{1}{3}B_s + \frac{(1-2e)c^2 + (1-e)^2 + e^2}{[(1-e)^2+e^2]c^2}\tfrac{1}{3}B_c, \end{aligned}\right\} \tag{3.7}$$

where these are again formal expressions in the sense of (3.6).

The normal velocity condition serves to eliminate the B's in favour of δ:

$$A_s + \frac{B_s}{3c^2} = \frac{e}{c}(\tilde{A} + \tilde{B}), \quad A_c + \frac{B_c}{3c^2} = \frac{e}{c}(\tilde{A} - \tilde{B}), \tag{3.8}$$

which, together with (3.6), imply that

$$B_s = \frac{3c^2\delta}{1-c^2}\left\{1 + \frac{2e}{c(1-c^2)}\right\} + O(e^2), \quad B_c = \frac{6c\delta e}{(1-c^2)^2}(1-c^3) + O(e^2), \tag{3.9}$$

and the formal expressions are sufficiently unwieldy that I have kept only the significant (uniform) parts. {In fact, only the leading [$O(1)$] term of B_s enters the calculation of Ω_s.}

Finally one determines δ and α by using the force conditions. The second of (2.17) determines

$$\delta \sim \tfrac{1}{2}(1-c^2)\left[1 - 2\frac{e}{c}(1-c^2)^{-1}\right], \tag{3.10}$$

which agrees with Phillips' (1960) inviscid result when $e \to 0$. The viscous correction is new, and differs (quantitatively, only) from that reported for a free surface by Ruschak & Scriven (1976) and by RFG. The first of (2.17) gives

$$\alpha \sim 2e(1-c^3)/c(1-c^2), \tag{3.11}$$

a new result.

3.2. *The axisymmetric nonlinear solution*

The axisymmetric problem may be written in core co-ordinates as in RFG. It is shown there that the interior can support neither radial nor axial velocities, and that the azimuthal velocity, determined by Ekman matching conditions on the end walls, is

$$\hat{v}^{(1)} = -Nc^4/r^5, \tag{3.12}$$

where $N = [27(\frac{2}{3})^{\frac{1}{2}} - 20]/20 = 0{\cdot}102270384....$ This conclusion depends on the leading terms of A_s and B_s and is thus unchanged here.

The boundary-layer equations on $r = c$ are

$$\begin{gathered} -2\bar{\tilde{v}}^{(1)} + \bar{\tilde{p}}_r^{(1)} = -\hat{\mathbf{r}} \cdot [\overline{\mathbf{u}^{(0)} \cdot \nabla \tilde{\mathbf{u}}^{(0)} + \tilde{\mathbf{u}}^{(0)} \cdot \nabla \hat{\mathbf{u}}^{(0)}}], \\ 2\bar{\tilde{u}}^{(1)} - E\overline{\tilde{v}_{rr}^{(1)}} = -\overline{u^{(0)} \frac{1}{r}(r\tilde{v}^{(0)})_r} - \overline{\tilde{u}^{(0)} \frac{1}{r}(r\hat{v}^{(0)})_r}, \quad \bar{\tilde{p}}^{(1)} - E\bar{\tilde{w}}_{zz}^{(1)} = 0, \quad \bar{\tilde{u}}_r^{(1)} + \bar{\tilde{w}}_z^{(1)} = 0. \end{gathered} \tag{3.13}$$

These equations are to be solved subject to the no-slip boundary conditions derivable from (2.14), which will leave Ω_s undetermined. The latter is then found from the torque balance.

The right-hand side of (3.13) is a function of r only. The radial component can be absorbed into the pressure and need not be considered further now. In RFG the azimuthal component was $O(e)$ and did not intrude into the main problem. This is not true here, and a particular solution, $\bar{\tilde{v}}_p$, satisfying

$$E\bar{\tilde{v}}_{p,rr} = \overline{[\hat{u}^{(0)} + \tilde{u}^{(0)}]\tilde{v}_r^{(0)}} \tag{3.14}$$

is required. (Only the dominant terms on the right-hand side are required.)

Putting $r = c - 2eR$ into (3.2), and using (3.8)–(3.10) to calculate the dominant parts of A_s, B_s, A_c and B_c, and noting that $\tilde{A} = 1 + O(e)$, $\tilde{B} = O(e)$, allows one to write the right-hand side, omitting terms of $O(e)$, as

$$(2c)^{-1}\{\exp R[(1+R)\cos R - R\sin R] - \exp 2R\}. \tag{3.15}$$

A first integral gives

$$\bar{\tilde{v}}_{p,r} = -(2ec)^{-1}\{R\cos R\exp R - \tfrac{1}{2}\exp 2R\}, \tag{3.16}$$

which takes the value $-(4ec)^{-1}$ on the boundary. The second integral gives

$$\bar{\tilde{v}}_p = -c^{-1}\{[R(\sin R + \cos R) - \sin R]\exp R - \tfrac{1}{4}\exp 2R\}, \tag{3.17}$$

which takes the value $(4c)^{-1}$ on the boundary.

The homogeneous solutions to (3.13) are the usual Stewartson layers as given, for this problem, in RFG. The associated azimuthal velocity can be separated into two parts, a z-dependent part in the $E^{\frac{1}{3}}$ layer and a z-independent part in the $E^{\frac{1}{4}}$ layer. As the particular and interior solutions are both z-independent, only the component in the $E^{\frac{1}{4}}$ layer is of direct interest.

This term can be written

$$\bar{\tilde{v}}_{\frac{1}{4}}^{(1)} = W_0 \exp \gamma_0(c-r), \tag{3.18}$$

where $\gamma_0 = (\lambda^2 E)^{-\frac{1}{4}}$. The leading terms in the (z-independent) stress condition, which condition comes from (2.18), are

$$-\gamma_0 W_0 - (4ec)^{-1} = 0, \tag{3.19}$$

from which $$W_0 = -(4ec\gamma_0)^{-1} = O(E^{-\frac{1}{4}}) \tag{3.20}$$

which will dominate the observed retrograde rotation. [If $(\lambda^2 E)^{\frac{1}{4}}$ is not small compared to c, as will be the case for the only experiments in the literature, (3.19) must be modified. This is discussed in § 4 below.]

4. Some experimental observations

The simplest experimental check one is tempted to make is to measure the retrograde rotation. Greenspan measured the straw rotation rate, from which one can infer the retrograde rotation rate. As I will show, Greenspan's data are inadequate to distinguish between the theoretical result and that given here, so I have also done an experiment which I report below.

In both Greenspan (1976) and the experiments reported here, the ratio of c to $E^{\frac{1}{4}}$ is not so far from unity that $E^{\frac{1}{4}}$ can be neglected in comparison with c. Thus, before I can use my theory to predict experimental results, a small correction must be made.

The shear stress balance in (3.19) is an asymptotic balance in which

$$\frac{1}{2}\left(\frac{1}{r}u_\phi + v_r - \frac{1}{r}v\right) \approx \tfrac{1}{2}\tilde{v}_r,$$

and the right-hand side is replaced by its dominant term, that in the $E^{\frac{1}{4}}$ layer. When $c = O(E^{\frac{1}{4}})$, the term v/c is equally important, and one should replace (3.19) by

$$-\left(\gamma_0 + \frac{1}{c}\right)W_0 - (4ec)^{-1} = 0, \tag{3.19}'$$

which gives

$$W_0 = -[(1+\gamma_0 c)(4e)]^{-1}. \tag{4.1}$$

No other change arises, as the stress associated with the inviscid interior flow is still small compared to that arising from the particular solution; W_0 dominates the retrograde flow.

Predictions of retrograde rotation are:

From Greenspan (1976)

$$1 - \Omega_s = \frac{\alpha^2 E_G^{-\frac{1}{2}}}{2\sqrt{2}}. \tag{4.2}$$

From this paper:

$$1 - \Omega_s = \frac{\epsilon^2}{4ec}[1 + c\gamma_0]^{-1} = \frac{\alpha^2 E_G^{-\frac{1}{2}}}{2\sqrt{2}} \frac{(\lambda^2 E)^{\frac{1}{4}}}{c + (\lambda^2 E)^{\frac{1}{4}}}. \tag{4.3}$$

(Recall that $\alpha = \epsilon/c$ and $E_G = E/c^2$ are the basic small parameters used by Greenspan.) There is a difference between (4.2) and (4.3) of a factor of

$$\frac{(\lambda^2 E)^{\frac{1}{4}}}{c + (\lambda^2 E)^{\frac{1}{4}}}; \tag{4.4}$$

formally the present result is $E^{\frac{1}{4}}$ smaller.

The difference is explicable in terms of the basic analyses in both papers, and the present result can be obtained using the reasoning in Greenspan (1976). That reasoning is that: (1) the velocity of the fluid at the straw must equal the velocity of the straw; (2) the net torque on the straw must vanish in the steady state; (3) the dominant

contribution to the torque on the straw is that from the particular solution. From these Greenspan obtains an integral condition which, in the notation used here, reduces to

$$\Omega_s = 1 - \epsilon^2/4ec,$$

which in Greenspan's notation is

$$\Omega_s = 1 - \alpha^2 E_G^{-\frac{1}{2}}/2\sqrt{2}, \tag{4.5}$$

his result.

One modifies the thought process by adding the $E^{\frac{1}{2}}$ layer. Then the continuity of (z-independent) velocity is given by

$$W_0 + \bar{\bar{v}}^{(1)} + \bar{\bar{v}}_p^{(1)} = \frac{e}{\epsilon^2}[\Omega_s - 1] \tag{4.6}$$

so that

$$W_0 = \frac{c}{\epsilon^2}[\Omega_s - 1] - \bar{\bar{v}}^{(1)} - \bar{\bar{v}}_p^{(1)} \tag{4.7}$$

and the torque condition gives

$$-\gamma_0 W_0 + \bar{\bar{v}}_{p,r}^{(1)} = 0, \tag{4.8}$$

from which

$$1 - \frac{\Omega_s}{\Omega} = \epsilon^2 \left[\frac{1}{4ec^2\gamma_0} - \frac{\bar{\bar{v}}^{(1)}}{c} - \frac{\bar{\bar{v}}_p^{(1)}}{c}\right] \sim \frac{\epsilon^2}{4ec^2\gamma_0}, \tag{4.9}$$

which is the result obtained in this paper (without the small c correction).

Before presenting my experiments, a brief assessment of Greenspan's experiment is appropriate. He gives the rotation rate of the straw as a function of the rotation rate of the container at six different values of c. No formal error estimates are given. I have taken the data from figure 4 in Greenspan (1976) graphically. The errors introduced by this process are less than 1 %, and probably small compared to distortions in reproduction which are, in turn, likely to be at most of the order of the true errors.

Figure 2 shows

$$K = (1 - \Omega_s) r_i \Omega^{-\frac{1}{2}}/(\Delta\rho)^2 \tag{4.10}$$

as a function of r_i, where r_i is the dimensional inner radius, equal to ac. Here

$$\Delta\rho = (\rho_f - \rho_s)/\rho_f,$$

where ρ_f, ρ_s denote the density of water and the mass of the straw divided by its volume, using the values given by Greenspan (1976).

For r_i in cm and Ω in 1000's of rev/min, Greenspan predicts that $K = 0{\cdot}289$, independent of r_i and Ω. This paper predicts that

$$K = 0{\cdot}0116 \frac{\Omega^{\frac{1}{2}}(\lambda^2 E)^{-\frac{1}{4}}}{1 + c(\lambda^2 E)^{-\frac{1}{4}}},$$

with Ω measured in 1000's of rev/min. The solid line in figure 8 is Greenspan's (1976) result and the dashed line that of the present work, with $\Omega = 1500$ rev/min. (The experiments vary from about 1000–2400 rev/min; as the expression depends only on the fourth root it seems silly to worry about a band of results.)

The data points were obtained by calculating K at each r_i using the mean of the observed values of $1 - \Omega_s$. The error bars depicted represent $\pm$ twice the sample standard deviation, calculated according to the small sample rule:

$$s^2 = \frac{1}{n-1} \sum_{i=1}^{n} (K_i - \bar{K})^2.$$

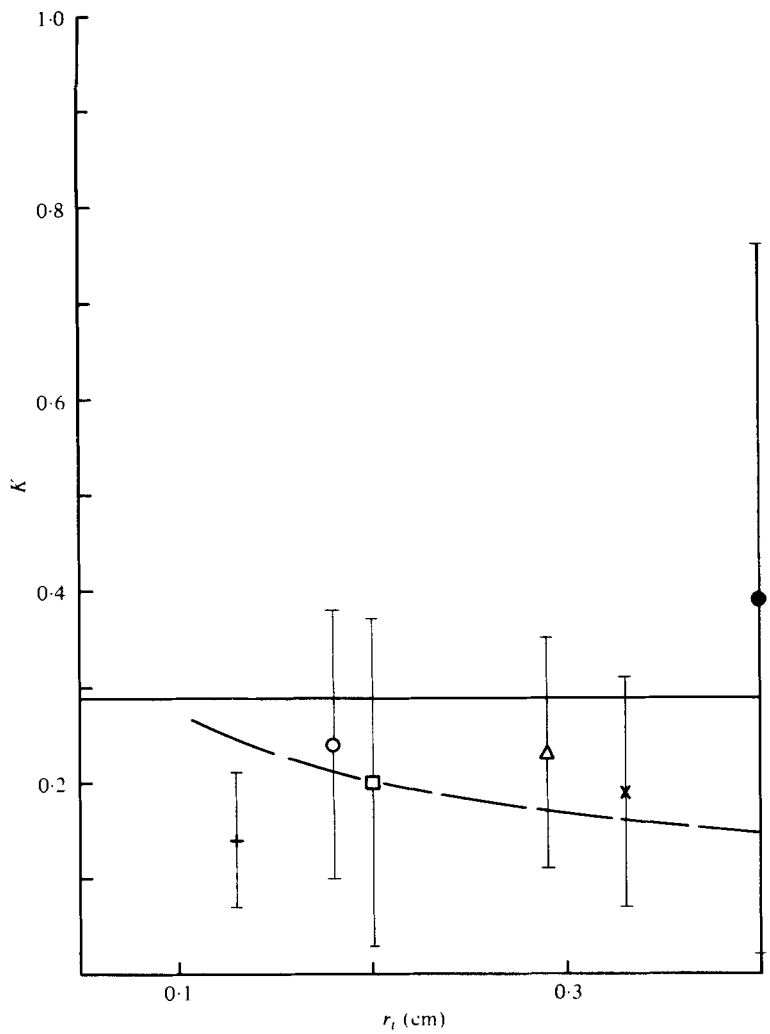

FIGURE 2. K [defined by (4.4)] *vs.* inner radius for the experiments in Greenspan (1976) (solid line): ●, $c = 5{\cdot}26 \times 10^{-2}$; ×, $c = 4{\cdot}34 \times 10^{-2}$; △, $c = 3{\cdot}82 \times 10^{-2}$; □, $c = 2{\cdot}63 \times 10^{-2}$; ○, $c = 2{\cdot}37 \times 10^{-2}$; +, $c = 1{\cdot}71 \times 10^{-2}$. ---, present paper.

Because of the experimental errors, and the asymptotic nature of the theories, one cannot make a stronger statement than: these data suggest that the present theory is to be preferred over that of Greenspan. [The results in Wood (1977) would give $K = 0{\cdot}145$, a result consistent with the data.]

The major problem in using Greenspan to distinguish among the theoretical predictions is that the ratio given by (4.4) is not sufficiently different from unity. It is hard to make E much smaller than 10^{-6}, a typical value in Greenspan's experiments, so one is left with the option of making c larger. Greenspan's c's range from $1{\cdot}71 \times 10^{-2}$ to $5{\cdot}26 \times 10^{-2}$. To obtain a dramatic contrast I built a float with $c = 0{\cdot}24$.

My experiments were performed in an acrylic cylinder with the inside dimensions of length = 184 mm and diameter = 158·8 mm, capable of rotation rates up to 1375 rev/min. My float was constructed of PVC drain pipe, capped with plastic ends.

It was a not quite circular cylinder having a major axis of 38·61 mm and a minor axis of 37·72 mm, determined by direct measurement using a vernier calliper. The overall length was 176 mm. Its mass was 47·5 g, giving an effective density of 0·236 g/ml and a $\Delta\rho = 0{\cdot}764$. I used a volume ratio to calculate $c = 0{\cdot}240$. The remaining parameter, $\lambda = 1{\cdot}16$. ($\lambda = 1{\cdot}25$ for Greenspan's experiment.)

A major problem in modelling a rigid free surface by a float is the interaction between the end walls of the float and the container. For thin straws ($c \ll 1$) this is probably not important. For the larger float I built it raises concern. I chose the length of the float to be small enough to allow several boundary-layer thicknesses between it and the container at each end. I do not know how effective this is. Intuitively, I expect the effect to be to *decrease* the retrograde rotation rate, that is, to make the float rotate more closely to the container rotation rate.

I measured the differential rotation period of the float as a function of the rotation rate of the container. I used a strobotach to 'freeze' the container in the laboratory frame. This provided a value for the rotation rate. I then observed the apparent rotation rate of the float by timing several rotations with a stop watch. For the more rapidly rotating cases I would time ten rotations; in slower cases I would take enough rotations to obtain total elapsed times in the range of 25–40 s. In no case were fewer than three rotations used. At each container rotation rate I repeated this timing exercise ten times.

The major source of experimental error is determining an integral number of rotations. I observed the passage of a mark on the float past a mark on the cylinder, and I may have made errors as large as one-fourth of a rotation period, leading to a maximum estimated error of one-fourth of a period divided by the number of periods timed. Thus, the fewer the periods timed, the larger the expected error.

I formalized the error by making ten measurements at each rotation, calculated the mean and standard deviation (using the small sample formula) and divided by the number of periods in a measurement. I used twice this sample standard deviation as a formal error. It is, of course, a measure of precision.

Figure 3 is a logarithmic plot of the differential rotation period as a function of container rotation rate. The two solid lines are theoretical: the upper left is that calculated from this paper and the lower right that calculated from Greenspan (1976). The error bars are the formal error described above; where none are shown, they would fall within the circles.

These data were taken on four different days. Some of the scatter is likely to be related to differing amounts of unwanted air in the container, and its distribution. There was usually a small air column visible between the float and the container at one or both ends, the diameter of which was roughly half that of the float. In addition there were always some air bubbles on the float's surface. Some of this air was sucked in from a faulty axial valve and the rest came out of solution from the water. A typical total air volume was 5–10 ml.

The reader is reminded that the small parameter arising from linearization *decreases* to the right. One expects better agreement in the upper right than the lower left. In addition the theoretical results are asymptotic in small fractional powers of the Ekman number. For the upper half of the data swarm, roughly those points above a container rotation rate of 900 rev/min, the present theory underestimates the differential rotation period (and hence overestimates the differential rotation) by

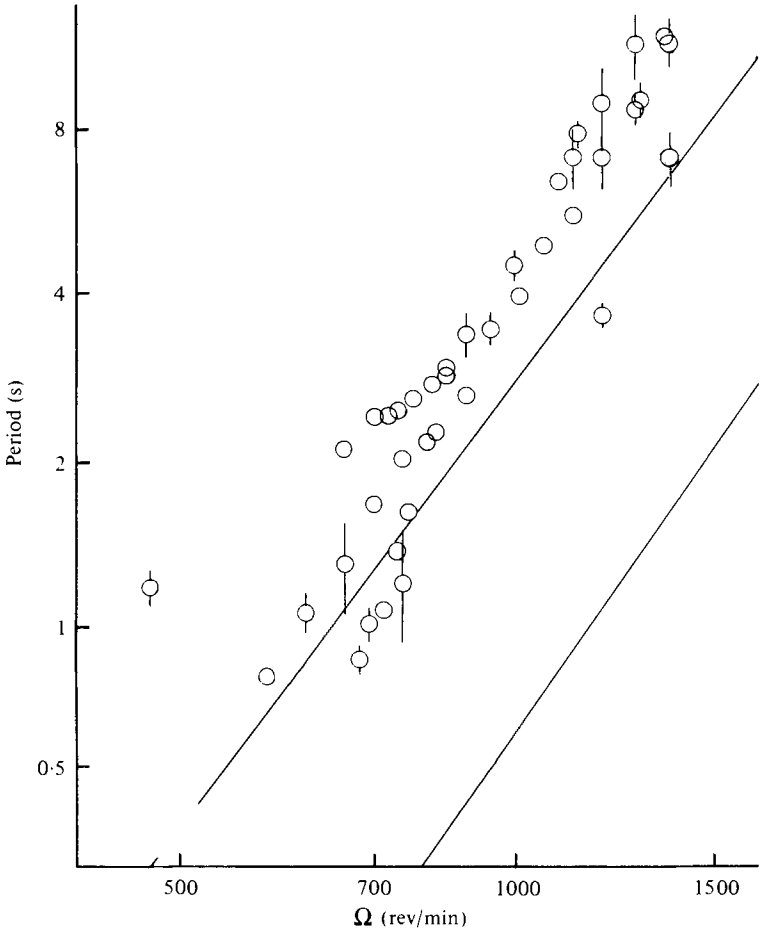

FIGURE 3. Retrograde rotation period *vs.* container rotation rate: $c = 0{\cdot}240$, $\Delta\rho = 0{\cdot}764$, $\lambda = 1{\cdot}16$. Upper solid curve is based on (4.3), lower on (4.2).

about 40 per cent. The theory in Greenspan (1976) is considerably worse. In view of the difficulties involving the end wall interactions and air infiltration, the fact that the discrepancy is less than ten times $E^{\frac{1}{4}}$ is heartening. I think it fair to conclude that the theory in Greenspan is probably inapplicable to containers with $\lambda = O(1)$, and that the theory presented here is in its essentials correct.

The flow is clearly more complex below 900 rev/min. Clearly more than one flow state is possible at a given container rotation rate. The data suggest to me a bifurcation at about 900 rev/min, and a second bifurcation on the lower branch at about 800 rev/min. I think the point at the far left belongs on the upper branch, and I spent some time trying to fill in the space between that point and the rest of the upper branch without success.

Both lower branches end at a period of about 0·9 s. Below this vortex shedding of the type described by Greenspan is observed, and the interface rotation becomes time-dependent, reading a (retrograde) maximum just before vortex shedding. I have made some very crude preliminary observations not suitable for reporting at this time.

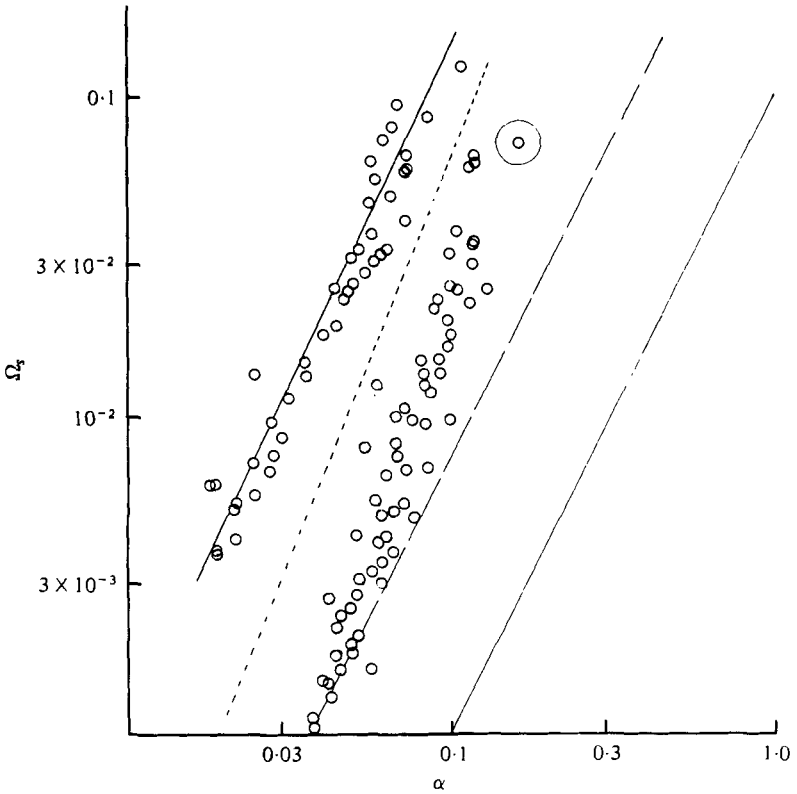

FIGURE 4. Retrograde rotation rate *vs.* α. Points above small-dashed line (and the circled point) are for a rigid interface with $c = 0{\cdot}24$; points below the small-dashed line are for an air–water interface for seven values of c between 0·10 and 0·20. The long-dashed line is taken from Whiting (1978) and represents an experimentally derived rotation rate for air–water and air–glycerol interfaces. The upper solid line is based on (4.3) in this paper. The lower solid line is based on the free surface theory given by Gans (1977).

I remarked in the introduction that Whiting's data for air–water and air–glycerol/water interfaces disagreed sharply with my theoretical predictions for an ideal free surface. It is of some interest to compare these data with the rigid interface data. This is done in figure 4, showing $1 - \Omega_s$ as a function of $\alpha\,(= \epsilon/c)$. The points above the small dashed lines (and the circled point) are the data from figure 3. The other points are data I took using various air cores in water, and timing the rotation periods of small bubbles on the interface. I used the same technique as I described above except that I froze the bubbles in the laboratory frame and timed the apparent container period. This was done because: (1) it is hard to tell one bubble from another as it goes around; (2) there was observable differential motion on the surface.

I have not drawn the formal errors on this figure because it is complex enough as it is. They are comparable to those in figure 3, and in no case come near violating the small-dashed line.

The long-dashed line is taken from Whiting. I have taken his empirical expression, which involves the sizes of the particles he used as markers and the viscosity, and let the marker particle size and viscosity go to zero. The resulting curve is the straight line I have drawn. My data are consistent with his.

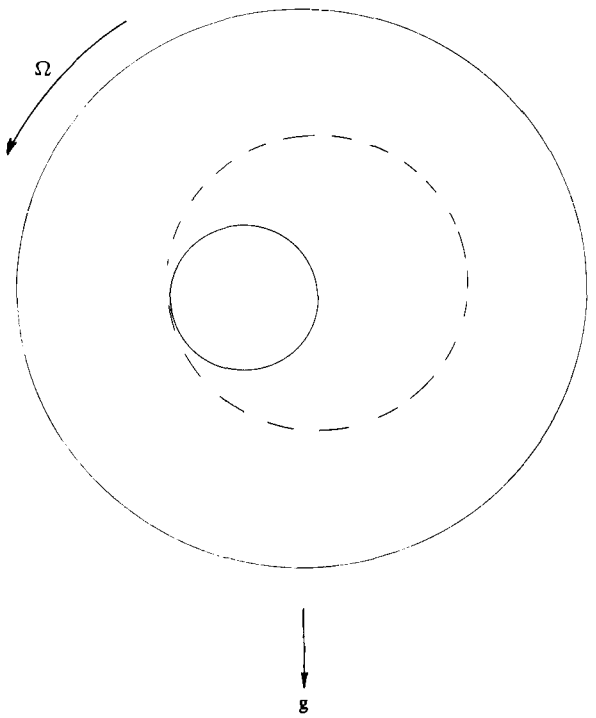

FIGURE 5. Intermediate spin-up stage. This drawing is schematic.

The upper solid line is derived from the theory given above. The lower solid line is derived from my ideal free surface theory. A possible interpretation of figure 4 is that the air–water interface has some effective rigidity; it can support some shear stress. Work addressing this point is in progress.

A final observation concerns spin-up from rest. At rest the float is at the top of the cylinder. When spun-up, the float is near the centre, moving as described above. The process by which the float–fluid system spins up is interesting to watch.

Initially the float begins to rotate and moves away from the wall in a prograde spiral until it reaches the position shown in figure 5. In that position it does not rotate. Its major axis is horizontal. It pitches and bobs vertically. The volume within the dashed circle is relatively quiescent. Small air bubbles stirred up by the initial phases of spin-up appear uniformly distributed within the region.

From time to time the float will rotate abruptly one half, or several half times. These episodes occur more frequently and last longer. The impression is of the outer fluid dragging more and more frequently on the float. Finally it rotates continuously, fairly slowly, and moves to its final position, where it spins rapidly up to its final rotation rate. It is during the latter rapid spin-up that markings on the float blur out of sight.

It spins down to rest by sliding sideways to the intermediate position, and then arcing directly to the top.

If the container is spun up impulsively and slowed (not stopped) before the float can spin up, the float moves to the centre and appears to spin up.

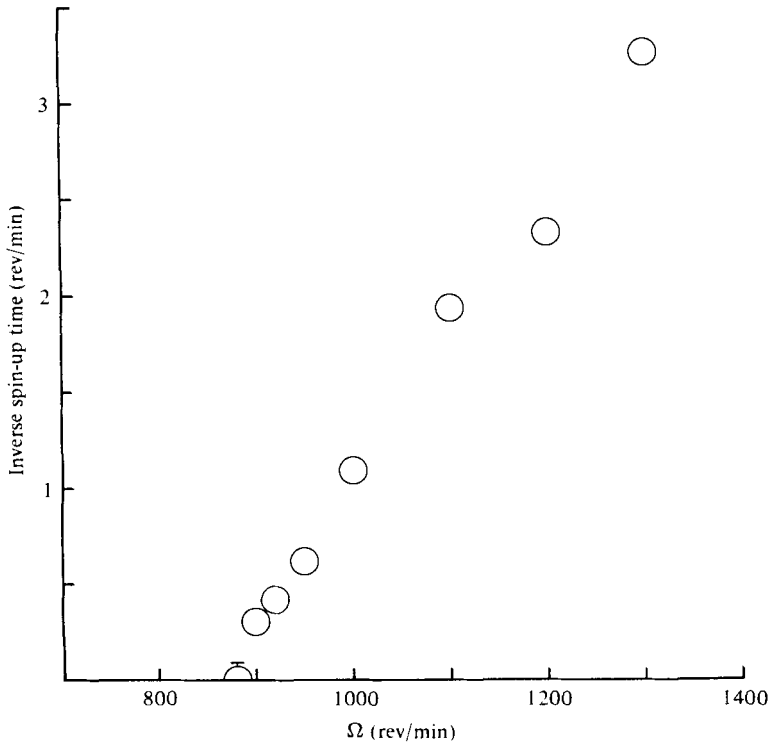

FIGURE 6. Inverse spin-up time *vs.* container rotation. The error bar on the point straddling zero indicates failure to spin up in 11 min, 0·09 on the ordinate.

I made some casual measurements of a spin-up time, which I defined as the time between the start of the cylinder and the final rapid spin-up of the float. This is not a well-defined interval and I was surprised how regular and simple a relationship is indicated. In figure 6, I show the spin-up frequency in rev/min [60/(spin-up time in seconds)] *versus* the rotation rate.

I offer no explanation for any of the spin-up data, but put it forward for whatever interest it may have.

I am grateful to the editor and a referee for pushing me into my laboratory. Without their encouragement the data I report here would not exist. Support from the Atmospheric Research Section of the National Science Foundation is gratefully acknowledged.

REFERENCES

GANS, R. F. 1977 On steady flow in a partially filled rotating cylinder. *J. Fluid Mech.* **82**, 415.

GREENSPAN, H. P. 1976 On a rotational flow disturbed by gravity. *J. Fluid Mech.* **74**, 335.

LANDAU, L. D. & LIFSCHITZ, E. M. 1959 *Fluid Mechanics*. Reading, Mass.: Addison-Wesley.

PHILLIPS, O. M. 1960 Centrifugal waves. *J. Fluid Mech.* **7**, 340.

RUSCHAK, K. J. & SCRIVEN, L. E. 1976 Rimming flow of liquid in a horizontal rotating cylinder. *J. Fluid Mech.* **76**, 113.

Whiting, R. D. 1978 An Experimental Study of Steady Flow in a Partially-Filled Cylinder. Ph.D. Dissertation, Department of Mechanical and Aerospace Sciences, University of Rochester, N.Y.

Wood, W. W. 1957 The asymptotic expansions at large Reynolds numbers for steady motion between non-coaxial cylinders. *J. Fluid Mech.* **3**, 119.

Wood, W. W. 1977 Torque-free rotation of a cylinder. *Phys. Fluids* **20**, 1953.